A Compact, Lightweight Robotic Ankle-Foot Prosthesis

Featuring a Powered Polycentric Design

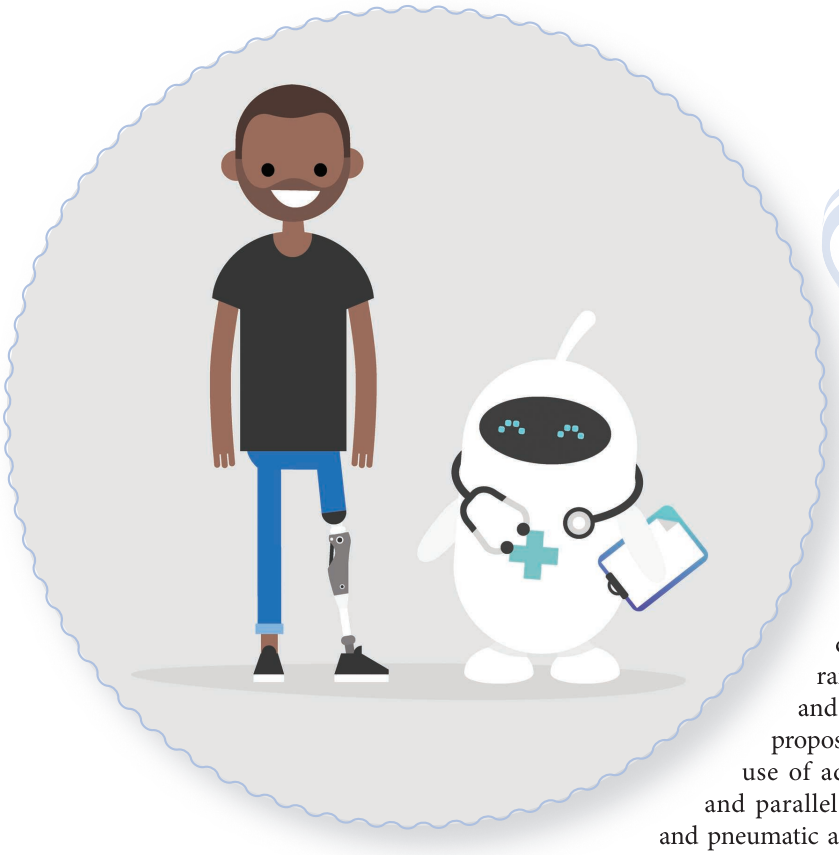

©ISTOCKPHOTO.COM/NADIA_BORMOTOVA

By Lukas Gabert, Sarah Hood, Minh Tran, Marco Cempini, and Tommaso Lenzi

Robotic ankle-foot prostheses aim to improve the mobility of individuals with below-knee amputations by closely imitating the biomechanical function of the missing biological limb. To accomplish this goal, they must provide biomechanically accurate torque during ambulation. In addition, they must satisfy further requirements such as build height, range of motion (ROM), and weight. These requirements are critical for determining the potential number of users, range of activities that can be performed, and clinical outcomes. Previous studies have proposed addressing this challenge through the use of advanced actuation systems with series and parallel elastic actuators, clutchable leverages, and pneumatic artificial muscles. These advanced actuation systems have shown improved mechanical and electrical efficiency compared to conventional servo motors, making powered ankle prostheses possible. However, the improved efficiency comes at the expense of a tall build height, reduced ROM, and significant increase in weight, thus limiting the clinical viability of currently available powered prostheses.

In this article, we show how a polycentric design can enable a lightweight powered ankle prosthesis to fit within the anatomical foot profile while providing physiological torque, energy, and ROM. Our simulations demonstrate that the moving instantaneous center of rotation (ICR) of the proposed polycentric mechanism has a twofold effect. It improves electrical efficiency by affecting the torque and speed required at the motor output and reduces the load on the main transmission system. Using the proposed powered polycentric design, we developed the first powered ankle-foot prosthesis that fits within the biological

Digital Object Identifier 10.1109/MRA.2019.2955740
Date of current version: 20 January 2020

foot profile of the 50th percentile male adult (12-cm build height) and matches the weight of the 50th percentile female ankle/foot (1.3 kg in total weight, including battery and covers). Experiments with two below-knee amputee subjects show how the proposed powered polycentric prosthesis can provide physiological torque and speed as necessary to perform common ambulation tasks that require net-positive energy, such as walking and climbing stairs.

Challenges and Limitations

Lower-limb amputation severely limits functional mobility and quality of life. Below-knee amputations are the most prevalent, representing 71% of dysvascular amputations [1]. The simplest and most frequently used ankle-foot prosthesis solution for individuals with below-knee amputation consists of a carbon-fiber foot rigidly connected to the user's residual limb [2]. This solution is lightweight and robust but has very limited functionality because the biomechanical function of the missing biological ankle is approximated by the carbon-fiber foot as a simple stiffness element [3].

Robotic ankle-foot prostheses have the potential to improve ambulation by more closely imitating the biomechanical function of the missing limb.

More recently, ankle-foot prostheses have been developed with an ankle joint actuated by passive elements such as springs and dampers [4]. In some advanced devices, the mechanical impedance of the ankle can be actively controlled during the gait cycle to improve ambulation [5]. A fundamental limitation of these prosthetic technologies is that they cannot actively generate movements and inject net-positive energy into the gait cycle, which are critical functions of a biological leg [6]. Prosthesis users compensate for these deficiencies with their residual limb and contralateral leg, resulting in a slower, less efficient, and less stable gait compared to able-bodied individuals [7]. Other ambulation activities, such as climbing stairs and ramps or transitioning between sitting and standing, are more challenging for individuals with below-knee amputations using available passive prostheses than they are for able-bodied individuals [8]. Thus, improved prosthesis technologies are necessary to address the unmet needs of individuals with below-knee amputations.

Robotic ankle-foot prostheses have the potential to improve ambulation by more closely imitating the biomechanical function of the missing limb [9]. To realize this goal, a powered ankle-foot prosthesis must provide physiological torque, speed, and power in a compact and lightweight design that fits within the biological ankle-foot profile. Researchers have proposed addressing these design challenges with innovative actuation systems that combine passive and active components. For example, four-bar mechanisms can reduce the motor torque demand by providing a higher gear ratio for the ankle positions that require higher torque [10]–[12]. Similarly, adding a dorsiflexion spring in parallel to the ankle joint has been shown to reduce the required motor torque due to the physiological bias in ankle plantarflexion torque during walking [13]. Springs have also been added in series to the motor to reduce the mechanical power output at the motor level and provide shock absorption for the transmission system [13]. Recently, clutches and brakes have been used in combination with springs to reduce the required peak motor power [14]. These advanced actuation solutions enabled the development of the first commercially available powered ankle-foot prosthesis, the Ottobock Empower.

Despite the improvements in electrical and mechanical efficiency, currently available actuation solutions have significant limitations. For example, four-bar linkages are affected by the inherent tradeoff between linkage size and load. In addition, they have a limited usable ROM. As a result, ankle prostheses designed with four-bar linkages cannot fit within the foot envelope and must be placed vertically on the shank portion of the ankle-foot prosthesis [10]–[12], which results in a large prosthesis build height.

Parallel springs can be made relatively lightweight and small [15] but are typically optimized for walking, which requires a stiff dorsiflexion spring with an equilibrium point close to the neutral ankle position. Consequently, the ankle prosthesis cannot rest in a dorsiflexed position and negatively affects activities of daily living, such as ambulation on stairs, descending ramps, transitioning between sitting and standing, and comfortable, resting dorsiflexed positions for sitting and standing. An alternative design strategy, known as a *hybrid design*, seeks to reduce the prosthesis size and weight by powering only a subset of activities [16]–[18] or avoiding net-positive energy injection [19]–[22]. This design strategy relaxes the speed and torque requirements on the actuation, resulting in smaller and lighter prostheses; however, in contrast to fully powered prostheses, hybrid prostheses cannot assist users during all ambulation activities. Therefore, there is a tradeoff between the functionality of a powered prosthesis and the actuation size and weight.

The size and weight of a powered prosthesis affect its function and usability. The build height determines the portion of the amputee population that can use a powered prosthesis, specifically depending on the subject's height and residual limb length. Moreover, the prosthesis weight affects biomechanics and clinical outcomes negatively. For example, a larger prosthesis weight has been shown to increase metabolic energy cost [23], exacerbate stance time and swing time asymmetries [24], and increases hip effort [25] during walking. Thus, a compact and lightweight fully powered prosthesis is necessary to improve ambulation for most individuals with below-knee amputation.

We present the first fully powered ankle-foot prosthesis that fits within the biological foot profile of the 50th

percentile male adult and matches the weight of the 50th percentile female ankle/foot. The proposed powered prosthesis uses a polycentric design with a moving ICR. Polycentric designs are commonly used in passive prostheses to improve static stability [26], [27] and reduce the socket torque in combination with an actuation system [28]. In this article, we propose an alternative design approach that consists of optimizing the ICR path to engineer the relationship among the ground reaction force (GRF), prosthesis torque, and motor torque to reduce the prosthesis size and weight. This design approach allowed us to develop a powered ankle prosthesis that can support common ambulation activities while fitting within the biological foot envelope. A powered ankle-foot prosthesis with these characteristics is not currently available to individuals with below-knee amputations. Preliminary work related to the proposed powered ankle was presented at a conference on intelligent robots and systems [29].

Design

Design Objectives

The primary design objective of a fully powered ankle-foot prosthesis is to provide biomechanically accurate torque and power for common locomotion tasks, such as walking on level and inclined ground and climbing stairs. The prosthesis must also be able to bear the static and dynamic loads generated by the user while wearing the prothesis. These actuation and structural requirements are typically obtained from the analysis of healthy biomechanics [30]–[32]. Similar to previous studies [12], [13], [33], we selected 125 Nm as a target for the maximum, repetitive peak torque. This peak torque requirement should allow for a powered prosthesis to provide biomechanically accurate torque for subjects up to 95 kg, according to [30]–[32].

Although most powered prostheses are developed to match the weight of the missing biological leg, studies suggest that decreasing the weight of the prothesis may lead to improved comfort [34] and walking economy [23]. Thus, we aspire for the powered prosthesis's weight to match that of the 50th percentile biological female ankle/foot, which is 1.35 kg [35]. Notably, this weight objective is 38% lighter than the only powered ankle-foot prosthesis available on the market (i.e., 2.2 kg [36]) and is also lighter than its biological counterpart for 54% of the population. Furthermore, we intend for our powered prosthesis to fit within the anatomical ankle-foot profile of the 50th percentile male. This build height is 45% smaller than the only powered ankle-foot prosthesis available on the market [36]. In this way, a larger segment of the below-knee amputee population will be able to use a powered prosthesis compared to the number of those who currently do.

The additional functional requirements are related to prosthesis usability in real-world scenarios. A certified prosthetist must be able to fit users with the prosthesis using commonly available tools and knowledge. Thus, the prosthesis design must allow for adjustments to each subject's anthropometry using mechanical interfacing, height adjustment, and the alignment norms of the prosthetics industry, such as pyramid connectors and pylon interfaces. From a user perspective, a powered prosthesis must support a full day of use on a single battery charge. An American adult walks 5,100 steps per day on average [37]. The prosthesis battery, therefore, must have enough electrical energy to power 2,600 strides on a single charge.

Polycentric designs are commonly used in passive prostheses to improve static stability and reduce the socket torque in combination with an actuation system.

Conceptual Design and Dynamic Simulations

The proposed powered polycentric mechanism does not have a physical revolute ankle joint. The pylon and the foot are connected through a seven-bar mechanism with one degree of freedom (DoF), which combines one rotation and two translations in the sagittal plane (Figure 1). The rotation occurs around the ICR (yellow circle in Figure 1), which is located at the intersection of the directions of the linkages $\overline{R_1R_2}$ and $\overline{R_3R_4}$. The rotation around the ICR determines the angular position of the proposed polycentric ankle by defining the relative inclination of R_2R_3 with respect to R_1R_4 and, consequently, the shank angle with respect to the foot. Moreover, the location of the ICR changes with the angular ankle position, as depicted by the dashed curved line in Figure 1. The trajectory of the ICR determines two translations that, when combined with the ICR rotation, define the DoF of the proposed ankle mechanism. Finally, the prismatic joint P_1 actuates the ankle DoF by regulating the inclination of $\overline{R_1R_2}$. A comprehensive analytical model of the proposed polycentric ankle kinematics is provided in our previous conference paper [29]. The proposed

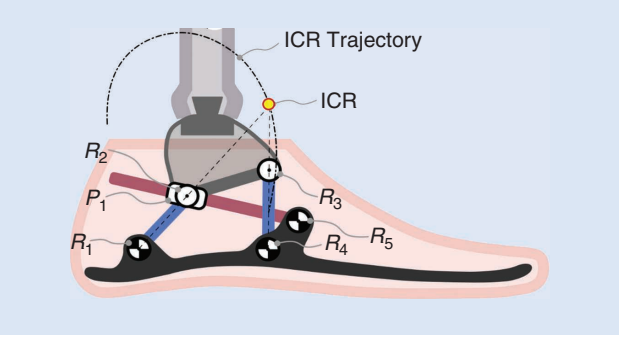

Figure 1. A schematic diagram of the powered polycentric kinematics, which shows the path of the ICR for the whole ROM as well as the mechanism's six joints.

polycentric mechanism has the potential to reduce the size and weight of a powered prosthesis.

Simulations were conducted to understand how the location of the ICR affects the ankle torque requirements during ambulation. The free-body diagram in Figure 2 shows that the torque in both polycentric and monocentric designs depends on the value of the GRF and its moment arm a_R (i.e., $T_{ICR} = GRF \cdot a_R$). However, the location of the ICR in the polycentric design differs from the anatomical location of the ankle. Hence, given the same GRF, the ICR torque of the polycentric design will be different from that of the torque in the monocentric design [Figure 2(b)], which has a fixed center of rotation similar to that of the anatomical ankle. The required joint torque profiles for a monocentric design (orange line) and the proposed polycentric design (blue line) are presented in Figure 3. Both profiles were obtained from a walking data set, including the GRF, center of pressure (CoP), and foot/shank inclinations [30].

The location of the ICR affects the loads on the linear actuator.

As seen in Figure 3(a) and (b), the monocentric ankle torque is biased in plantarflexion. The polycentric design reduces the torque bias by placing the ICR anterior to the monocentric ankle joint location. Consequently, the polycentric design has higher dorsiflexion torque and lower plantarflexion torque compared those of the monocentric design. The net result is a 14.5% decrease of the torque root mean square (rms) over the gait cycle. Note that both torque/angle curves show the same net-positive energy [Figure 3(a)] (i.e., the integral of the torque over the angular displacement). Thus, the polycentric design provides the same energy injection as that of a monocentric design with a lower-torque rms. This torque rms reduction is advantageous because it has the potential to lower the required motor current and heat generation, which limit the performance of a powered prosthesis [17].

The location of the ICR affects the loads on the linear actuator. As displayed in the free-body diagram in Figure 2, for both the polycentric and monocentric designs, the torque generated by the GRF is balanced by the linear actuator push-pull force (i.e., $T = GRF$ and $a_R = A \cdot a_A$). Hence, for a given torque (T), the load on the linear actuator (A) is inversely proportional to its moment arm (a_A). The bigger the moment arm (a_A), the smaller the force on the linear actuator (A). As shown in Figure 2(b) of the monocentric design, the moment arm of the linear actuator (a_A) is constrained by the physical dimensions of the device. For example, increasing the moment arm (a_A) requires an increase in the prosthesis size, while decreasing the moment arm (a_A) requires an increase in the loads on the linear actuator (A).

In contrast, the polycentric design [Figure 2(a)] can place the ICR outside the physical dimensions of the prosthesis, thus avoiding the tradeoff between physical prosthesis dimensions and the load on the linear actuator. Our biomechanical simulations [Figure 3(c)] demonstrate that the peak force on the linear actuator during walking is 34.1% lower for the proposed polycentric design than it is for a conventional monocentric design. Accordingly, the polycentric kinematics may enable a more compact and lighter design by decreasing the load on the linear actuator without increasing the physical dimensions of the prosthesis.

The net effect of the polycentric kinematics on the motor torque requirements can be quantified using dynamic simulations. Starting from the physiological GRF and CoP, we can compute the required joint torque, linear actuator force, and motor torque, including the dynamics of the transmission system and related energy losses. Hard limits on the motor speed-torque curve are included in the simulation based on the battery voltage (i.e., 22.2 V nominal), which was similar to that of our previous work [17]. As a benchmark for the proposed polycentric design, the same simulation framework can compute the required motor torque for monocentric designs without springs and with a dorsiflexion parallel spring (5 Nm per degree, as in [15]). Both monocentric designs use the kinematic configuration shown in Figure 2(b). In addition, both polycentric and monocentric configurations use the same electrical motor (EC 30 four-pole, Maxon Motors). Note that each

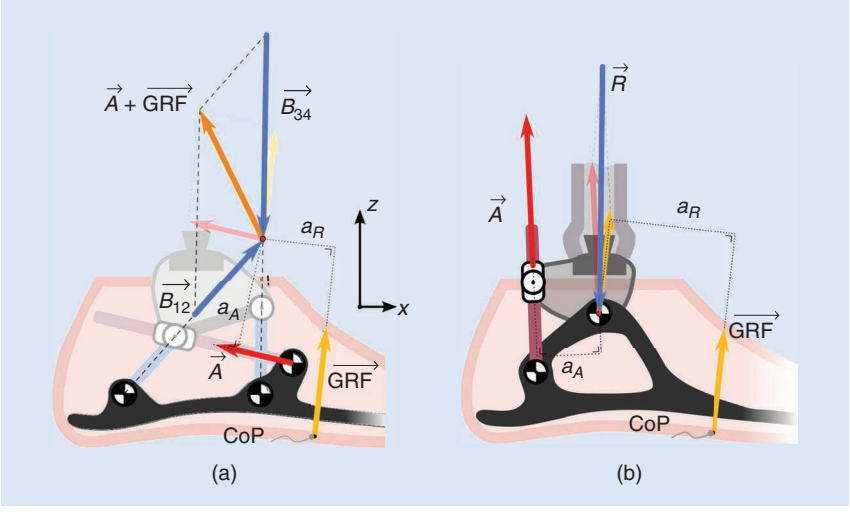

Figure 2. Free-body diagrams of (a) the proposed polycentric mechanism and (b) a monocentric design of a four-bar mechanism with a linear actuator of roughly the same volume. The GRF is balanced by the linear actuator force $\vec{A}$. The moment arm of the GRF with respect to the revolute joint location a_R determines the torque around the revolute joint for a given GRF. The moment arm of the linear actuator a_A determines the linear actuator force for a given torque around the revolute joint.

actuation configuration is simulated using the transmission ratio that minimizes electrical energy consumption.

Figure 4(a) shows that the proposed polycentric design (blue) requires similar motor torque to that of the monocentric design with a parallel spring (purple) and lower torque than that of the monocentric design without spring (orange). As seen in Figure 4(b), the motor current rms is 7.42, 12.33, and 7.31 *A* for the polycentric (blue), monocentric with no spring (orange), and monocentric with parallel spring (purple), respectively. In addition, the electrical energy consumption for a single stride was 33.6, 52.2, and 32.4 J for the polycentric, monocentric with no spring, and monocentric with a parallel spring, respectively. Thus, the electrical consumption of the proposed polycentric design is similar (i.e., + 3.7%) to that of a monocentric design with a parallel spring; however, because the polycentric mechanics do not require a

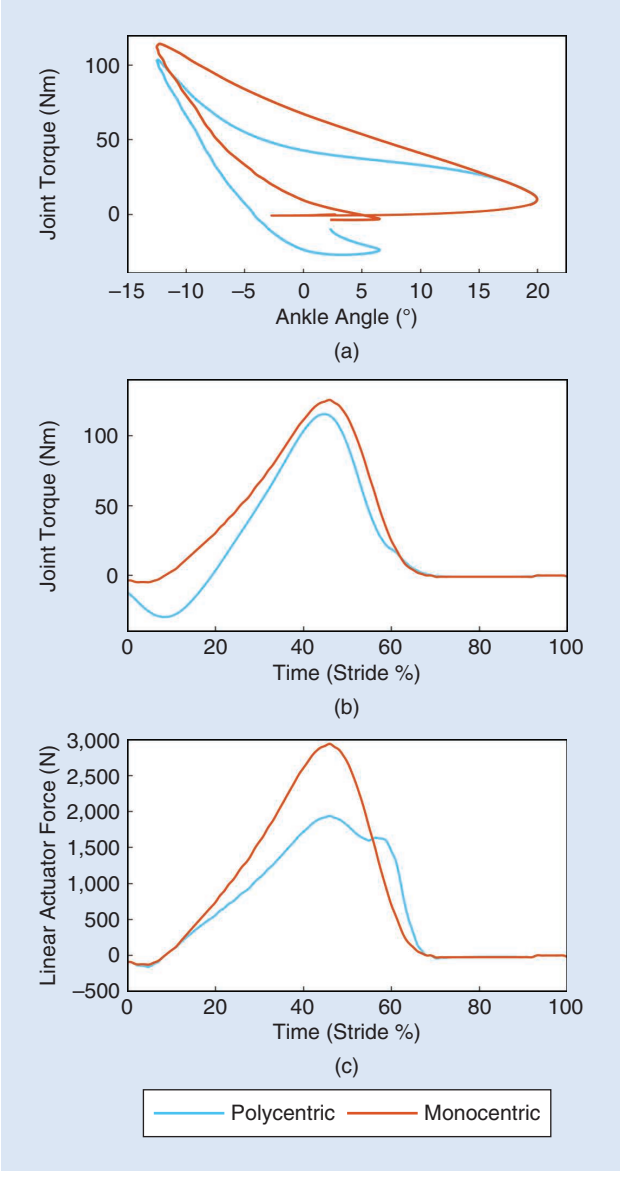

Figure 3. A comparison of the polycentric (blue) and monocentric (orange) ICR torque and linear actuator force during level-ground walking. Positive angles and torque represent plantarflexion, and negative angles and torque represent dorsiflexion. The quasi-stiffness curves show (a) that the polycentric design requires larger negative torque (i.e., dorsiflexion) and smaller positive torque (i.e., plantarflexion) compared to that of the monocentric design. The same trend can be seen by representing the torque as a function of (b) the normalized stride time (stride percentage). (c) An analysis of the linear actuator force during level-ground walking shows that the polycentric design requires a lower force compared to that of the monocentric design.

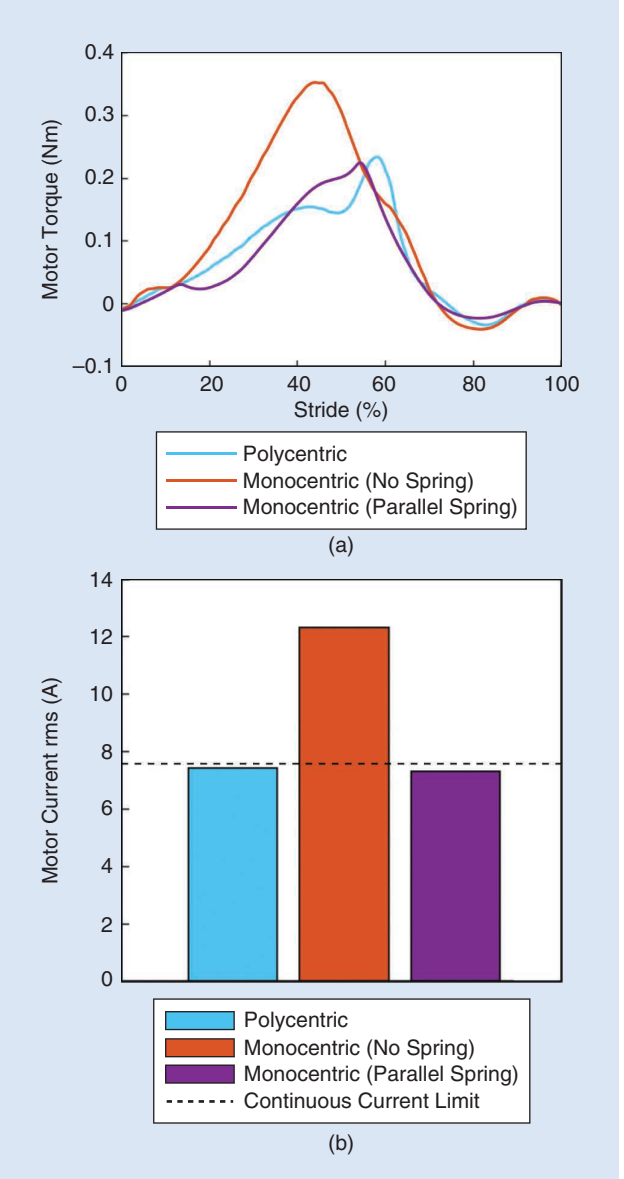

Figure 4. (a) Dynamic simulations show that the motor torque required to walk on level ground for the proposed polycentric design (blue) is similar to that required in a monocentric design with a parallel spring (purple) and significantly lower than a monocentric design without a spring (orange). (b) Further analyses show that the rms of the motor current exceeds the continuous motor current (dashed line) for the monocentric design without a spring (orange), suggesting that this design strategy is not feasible. The polycentric (blue) and monocentric design with a parallel spring (purple) have similar motor current rms values; therefore, they are expected to have similar electrical power consumption.

parallel spring, it can be made smaller and lighter while achieving a wider ROM in dorsiflexion.

Unlike a monocentric design, a polycentric mechanism produces a combination of rotational and translational movements. Consequently, the movement of the shank with respect to the foot differs between a polycentric and a monocentric design. These deviations are displayed in Figure 5(a) for the proposed design (orange line) compared to the "ideal" ankle rotation (black dashed line). Notably, translational movements affect gait dynamics when the foot is in contact with the ground during the stance phase [38], which may affect comfort, stability, and knee kinematics. In contrast, translational movements that occur when the foot is not in contact with the ground affect foot clearance, which is critical for prosthesis users [39]. The maximum deviation between a monocentric design (physiological ankle) and the proposed polycentric design is lower than 4.5 mm during the stance phase in level-ground walking [i.e., 0–60% of the stride in Figure 5(b)]. By comparison, deviations of up to 10 mm occur during the swing phase [i.e., 60–100% of stride in Figure 5(b)], thereby reducing the effective prosthesis height. Thus, the polycentric design has the potential to improve foot clearance compared to that of a monocentric design.

Actuation and Mechanical Structure

The side and front views of the powered polycentric ankle prototype without the protective foot shell are depicted in Figure 6. The proposed powered ankle-foot prosthesis comprises a polycentric structure, linear actuator, and custom carbon-fiber foot keel. The polycentric structure is made of aluminum 7075-T6. The revolute joints are realized by hardened steel shafts and polytetrafluoroethylene bushings. The linear actuator includes a brushless motor (Maxon Motors, EC four-pole 30, 24 V and 200 W), a roller screw (Rollvis, lead 2 mm, with a 90% efficiency), and a helical gear pair (custom machine from Boston-Gear H2412L and H2436R, 45° helix, and teeth ratio of 36:12). A low-profile custom carbon-fiber keel minimizes weight and build height. Similar to our previous work [17], we used an iterative design process based on the dynamic simulations and primary design objectives of motor efficiency, ROM, mechanism size, and projected overall weight. A biomechanics data set extracted from able-bodied individuals [30] provided the input for the simulations. An electromechanical model of the powertrain was

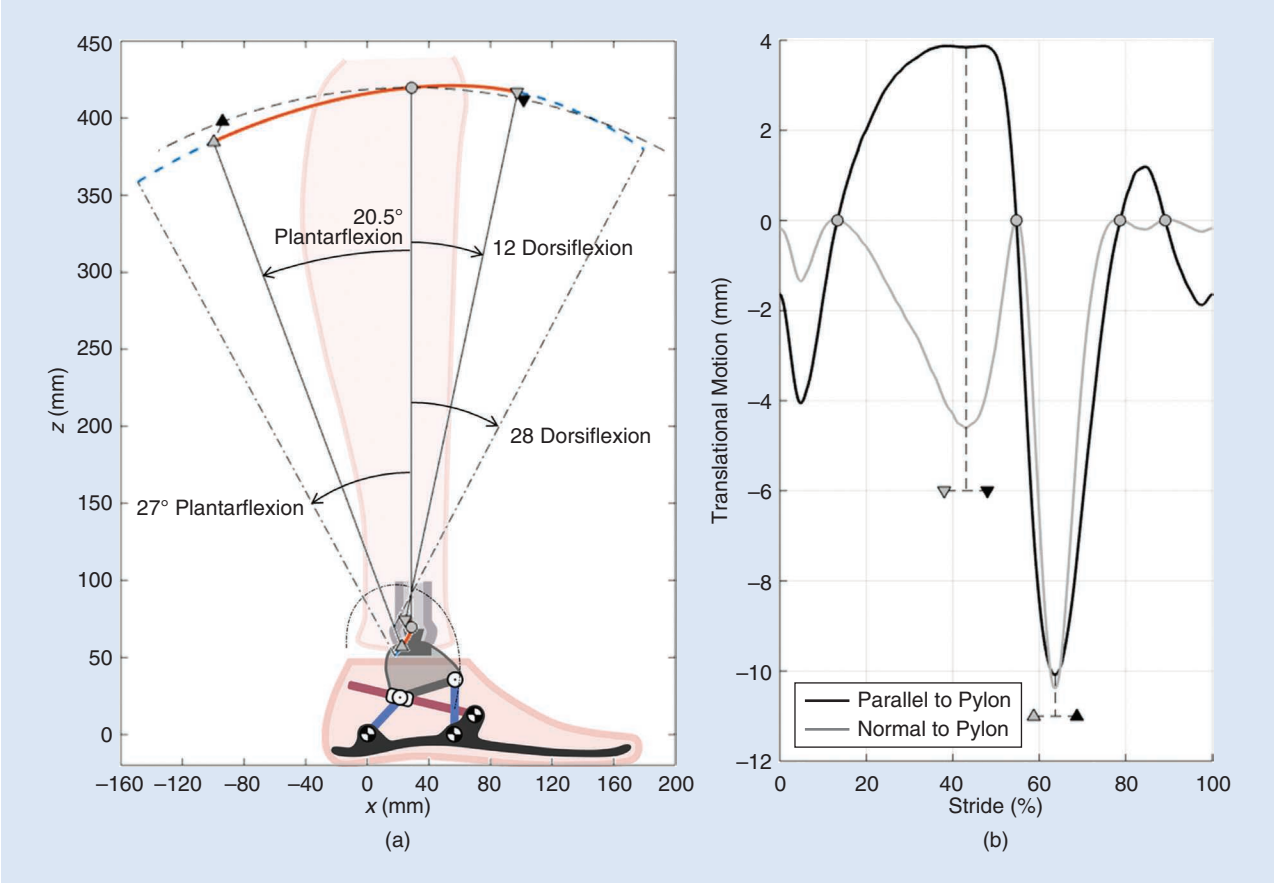

Figure 5. (a) The motion traces of the pylon center and a point 350 mm along the pylon (orange) approximate knee location with respect to the foot. The black dashed line represents an "ideal" rotation-only motion of the knee centered in the connector for a neutral ankle position. (b) The deviation of the trajectory from the physiological path within a level-walking stride in the directions parallel (black) and normal (grey) to the pylon axis (sagittal plane).

used together with the kinematic model described in [29] to select the appropriate motor, transmission, and linkages' dimensions. The powered polycentric ankle size and weight breakdown are reported in Figure 6(b) and Table 1, respectively.

Sensing and Electrical System

The powered polycentric ankle contains contactless sensors to estimate the position and velocity of the ankle joint. Specifically, an absolute magnetic encoder (RLS RM08 with linear voltage and a clockwise rotation of 90°) is located coaxially with the linkage $\overline{R_1R_2}$ and an incremental magnetic encoder (RLS, RM08, 512 counts per revolution) is located coaxially to the motor shaft. The two encoders provide independent estimates of the position and velocity of the ankle joint based on the geometrical model of the polycentric mechanism. These estimates are fused using a complementary filter to obtain the final measures of the ankle position and velocity for the control loops. This sensory fusion strategy combines the accuracy of the absolute sensor with the resolution of the incremental sensor, ultimately improving the position signal quality.

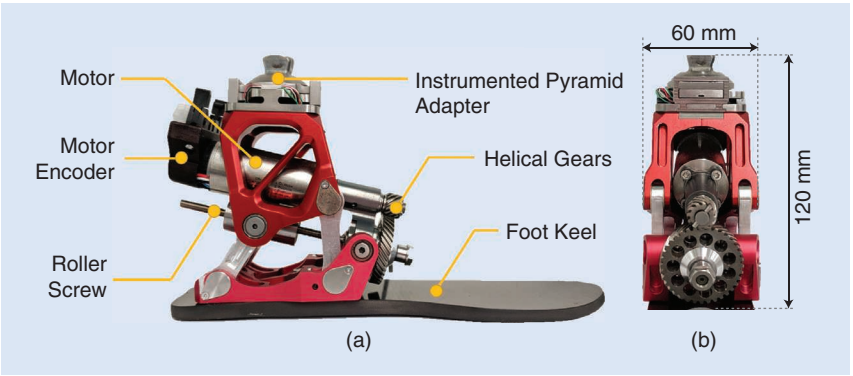

Figure 6. The (a) side- and (b) front-view photos of the powered polycentric ankle without the foot shell show the main prosthesis components, including the brushless motor with a custom encoder and connectors, primary helical-gear transmission, secondary roller screw transmission, custom carbon-fiber foot keel, and custom-instrumented male pyramid adapter. The height from the bottom of the foot keel to the top of the instrumented pyramid adapter is 120 mm. The maximum width of the powered polycentric prosthesis is 60 mm.

A custom-instrumented male pyramid adapter provides inertial and force/torque sensing as necessary to operate the high- and low-level controllers. The instrumented pyramid contains a nine-axis inertial measurement unit (IMU) (16-bit TDK MPU9250), which provides data on the prosthesis acceleration and angular velocity. The accelerations and velocity are further fused to estimate the inclination of the shank with respect to gravity. Furthermore, the instrumented pyramid provides information on the axial force and sagittal-plane torque through custom force-sensing elements based on Hall sensors. The pyramid has a full-scale range of 120 Nm and 2,500 N with a nonlinearity of 2.1 and 8.3% during ambulation, respectively. The instrumented pyramid communicates with the main controller using a high-speed inter-integrated circuit. The instrumented pyramid is described and characterized in detail in [40].

An overview of the electrical system for the powered polycentric ankle is shown in Figure 7. The prosthesis power supply is a 1,050-mAh, six-cell lithium-polymer battery. A 5-V regulator is used to scale the supply voltage as required to power the prosthesis processing units and embedded sensors. Two separate processing units are deployed to run the control routines and secondary functions, such as data logging and Wi-Fi communications. All time-critical routines, i.e., sensor reading, filtering, joint position, and torque control loops, run at 2 KHz on the joint controller unit (JCU) (Atmel MK20DX256). The JCU also communicates with the motor current servo controller (Elmo Motion Control G-TWI10/100SE) using pulsewidth modulation (PWM). The high-level control loops, data logging, and user communication operate on the coordination-control unit (CCU) (Raspberry-Pi model 3 A+) at 500 Hz. The CCU communicates with a laptop computer using Wi-Fi. The laptop runs a custom graphical user interface (GUI) for data monitoring and parameter-selection purposes. Hence, the GUI provides the experimenter with the ability to modify the ambulation mode and other ankle control parameters while the device is operating. The CCU communicates with the JCU over serial peripheral interface (SPI). The CCU and JCU are integrated with the current servo controller and the voltage regulator on a custom motherboard [Figure 7(b)]. The electrical system is fully enclosed in a custom protection cover and located on the socket to minimize build height and reduce the prosthesis' distal mass. The electrical power consumption is 3.8 and 3.1 W, respectively, with Wi-Fi on and off.

Table 1. The weight breakdown.

Weight Breakdown		
Motor with incremental encoder	300 g	Mechanics: 717 g
Transmission (roller screw, gears, and bearings)	187 g	
Four-bar structure (including bushing and fasteners)	230 g	
Foot keel	89 g	Interfaces: 239 g
Instrumented pyramid adapter	150 g	
Electronic Boards	135 g	Electrical: 365 g
Battery	186 g	
Cover	60 g	
Total weight	1321 g	

Control System

The proposed control system is based on a hierarchical architecture [41]. At the highest level, a finite-state machine determines which ambulation mode the user wants to perform. For each ambulation mode, a different midlevel controller is implemented. Finally, at the lowest level, a position controller and a torque controller are used in the swing and stance phases, respectively. For the goal of this article, the ambulation mode is manually selected by the experimenter through the GUI. Future work will focus on integrating automatic gait transitions using machine learning [41], electromyography [42], and computer vision [43].

In this article, we focus on walking and ascending stairs, as these ambulation activities require the powered prosthesis to provide net-positive energy and wide ranges of torque, speed, and ROM. The walking- and stair-ascent controllers are conceptually divided into stance and swing. In the stance phase, we impose a virtual impedance obtained from either quasi-stiffness profiles [44] or stiffness and damping values [41] extracted from able-bodied biomechanics [45]. Furthermore, we divide stance into two energetically passive phases and use the transition between these two phases to inject positive energy into the gait cycle. A finite-state machine is used to transition between stances 1 and 2 and the swing phase (Figure 8). The same finite-state machine is used for walking and stair ascent, although with different transition conditions and impedance parameters. In the swing phase, we use a minimum-jerk controller [46] to define a position trajectory that replicates the physiological ankle movement. The minimum-jerk trajectory is planned during the transition between stance and swing based on the current ankle position and velocity. Moreover, the duration of the swing trajectory is automatically adjusted to the user's cadence based on the duration of the previous stance phase.

A position controller [Figure 9(a)] is used during the swing phase to follow a desired trajectory. The position controller takes as input the desired position, velocity, and acceleration defined by the minimum-jerk midlevel controller. The desired position is compared to the measured ankle position, which is estimated using a complementary filter that combines the reading from the absolute encoder and the motor incremental encoder [Figure 9(c)]. The position error is fed to a

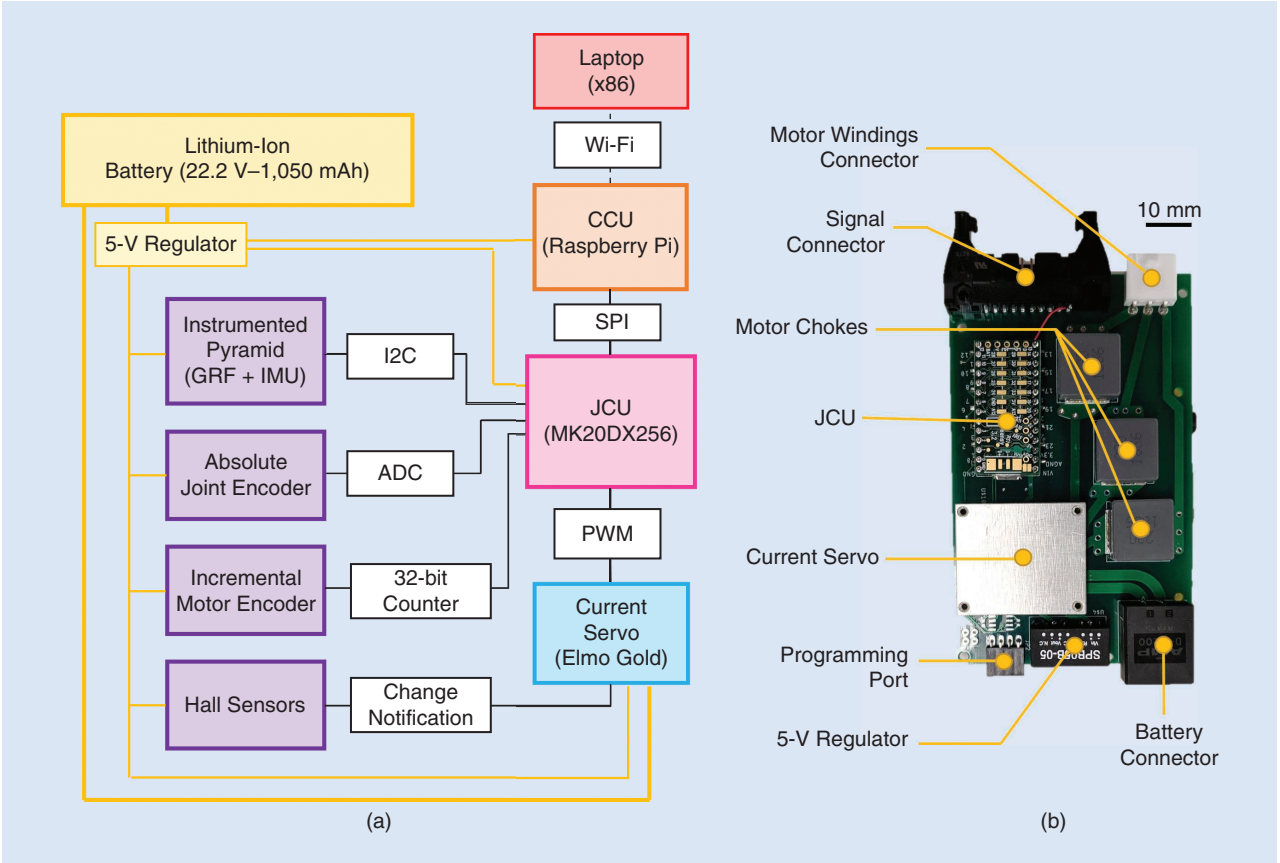

Figure 7. (a) An overview of the embedded system architecture and (b) a photo of the electrical system. The inputs for the joint controller unit (JCU) include an analog absolute joint encoder, an incremental motor encoder (quadrature count reading), and an integrated GRF/IMU sensor communicating over the inter-integrated circuit (I^2C). The JCU communicates with the current servo controller using PWM. The inputs to the current servo controller include the motor Hall sensors and emergency stop. In addition, the JCU communicates with the CCU through serial peripheral interface (SPI). In turn, the CCU communicates with a laptop computer over Wi-Fi for data monitoring and parameter-selection purposes. The CCU includes a secure digital card reader for data logging. All of the electrical components, with the exception of the CCU, are located on the same side of (b) the motherboard. ADC: analog-to-digital converter; mAh: milliamp per hour.

proportional-derivative (PD) controller that determines the feedback component of the ankle torque command. Moreover, the desired velocity and acceleration determine feedforward torque commands based on a dynamic model of the transmission system including its damping and inertia, which equal 3.5e-5 Nm s/° and 43.01e-7 kg m^2, respectively. These compensator parameters were found experimentally using the method described in [15]. The sum of the feedback and feedforward torque commands produces a desired motor torque value, which is sent to the motor driver [Figure 9(c)].

In the stance phase, a low-level torque controller is used to render a desired virtual impedance or quasi-stiffness, as computed separately by the midlevel controllers used for walking and stairs. The torque regulator comprises a feedforward command based on the position-dependent transmission ratio [Figure 9(b)]. In addition, two compensators are used to modify the transmission dynamics. The first takes as input the motor position measured by the incremental encoder to generate an online estimate of the viscous torque due to the linear actuator ($G_B(S) = s/(1 + 0.00796 \cdot s)$). The second takes as input the motor position and computes a scaled and low-pass-filtered estimate of the transmission inertia similar to that presented in [47], ($G_I(S) = (0.8 \cdot s^2/(s + 0.9556 + 0.0425i)(s + 0.9556 - 0.0425i))$). The coefficients of the compensators were determined experimentally. The purpose of these compensators is to reduce the apparent impedance (i.e., viscosity and inertia) of the transmission system to improve the fidelity of the virtual impedance controller [41].

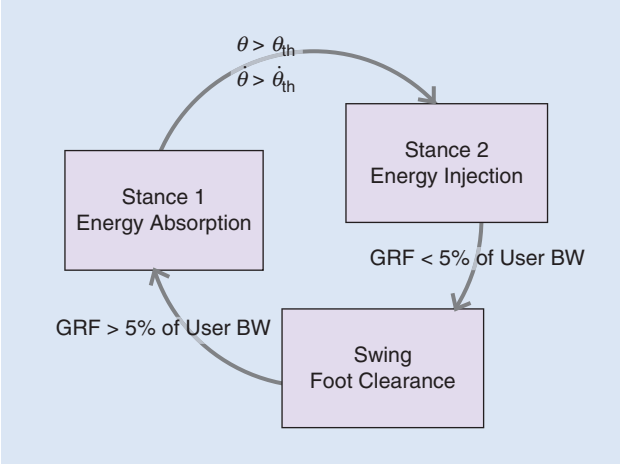

Figure 8. A block diagram of the finite-state machine used for walking and stair ascent. In stance 1, the prosthesis absorbs the impact with the ground, storing and dissipating energy as necessary. For the prosthesis to transition to stance 2, the ankle position must be greater than that of a specific dorsiflexed position, and the ankle velocity must be positive (i.e., ankle plantarflexing). The prosthesis injects net-positive energy into the gait cycle during stance 2. When the instrumented pyramid detects that the GRF is lower than 5% of the user's body weight, the controller transitions to swing mode. In swing, a minimum-jerk trajectory is executed, enabling the ankle prothesis to clear the ground and then prepare for the subsequent stance phase. When the GRF exceeds 5% of the user's body weight, the finite-state machine transitions to stance 1, initiating a new gait cycle. BW: body weight.

Comparative Analysis

A comparative analysis with other fully powered ankle prostheses is shown in Table 2. Only the Ottobock Empower (previously BIOM) and the Vanderbilt University (VU) ankle have embedded battery and electronics. The VU ankle [48] is the only one that uses rotational-only transmission, whereas all other devices use four-bar linkages with linear transmissions. The Walk-Run (from SpringActive) [49] and VU ankles use a very stiff foot keel that has minimal impact on the prosthesis's joint dynamics. The BIOM [13] and VU ankles [48] use a rather stiff

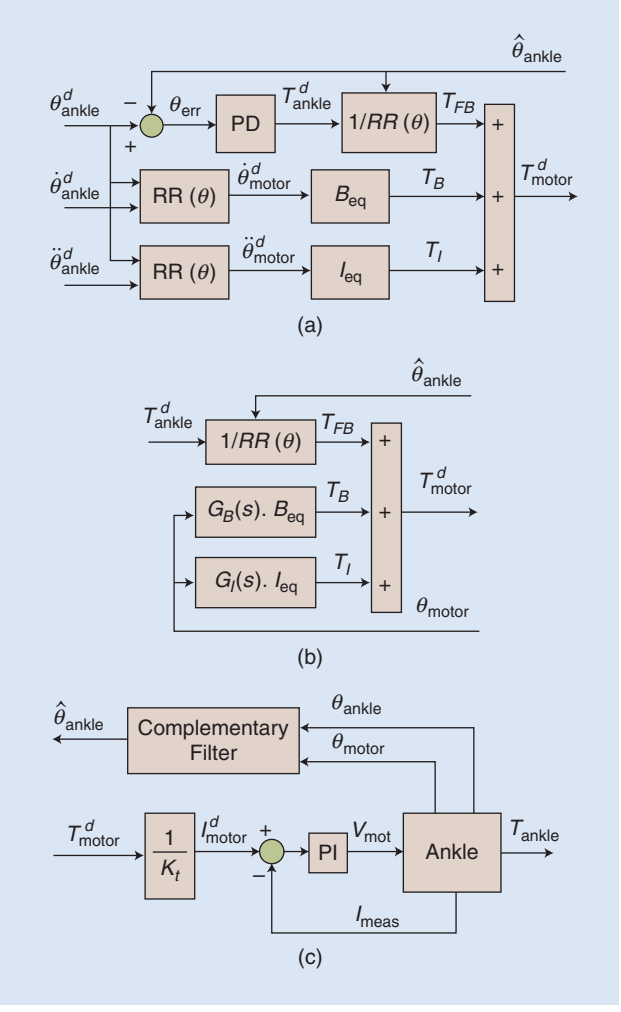

Figure 9. Block diagrams of the prosthesis low-level controllers and sensory fusion algorithm. (a) A closed-loop position control is used in swing mode to follow a desired trajectory. The proposed position controller comprises a PD feedback loop and two feedforward terms, which compensate for the equivalent damping and the inertia of the actuation system at the motor shaft. (b) During the stance phase, a sensorless torque controller is implemented with a feedforward term and two compensators, which use a filtered measure of the motor position as input. Both (a) the position and (b) the torque controllers produce a desired motor torque that is sent to the current servo driver, which runs (c) a closed-loop controller. The ankle angular position employed by the position and torque controller is estimated using a complementary filter, which combines the signals from the encoders located coaxially with the motor shaft and the polycentric mechanism. RR: reduction ratio; PI: proportional integral.

(~5 Nm per degree) parallel dorsiflexion spring to reduce the required motor torque/current during ambulation, thus improving electrical efficiency. However, the parallel spring reduces the ROM in dorsiflexion, which may negatively affect comfort and functionality for sit-to-stand transitions and stair ambulation. Comparing powered ankle prostheses without embedded battery and electronics shows that, at 956 g (Table 1), the powered polycentric ankle is 62, 50, and 50% lighter than the ankle-mimicking prosthetic foot, Walk-Run, and University of Massachusetts ankles, respectively.

As listed in Table 2, the powered polycentric ankle is lighter and has a lower build height than of any other fully powered ankle prosthesis. Placing the electrical system and battery pack on the socket (similar to the semiactive Össur PROPRIO FOOT [50]) is fundamental for improving build

Table 2. A powered ankle-foot prosthesis comparison.

Device	Build Height (cm)	ROM (Plantarflexion–Dorsiflexion) (°)	Rated Motor Power (W)	Top Speed (steps per min)	Peak Torque (Nm)	Weight (kg)
Empower and Ottobock (previously BIOM [13])	19	24–10+	200	100	125	2.2
VU leg, generation 3 (ankle only) [48]	21	45–30+	100	120	140	2.3
AMP-foot [33]	20	30–15	60	100	125	2.5*
Walk-Run [49]	30	30–10	200	150	140	1.9*
UMass ankle [38]	18.4	10–0	200	N/A	100	1.9*
Powered polycentric ankle	12	27–28	200	125	125	1.32

VU: Vanderbilt University; AMP: ankle mimicking prosthetic; UMass: the University of Massachusetts; N/A: not applicable.
* Without battery and electrical system.
+ Dorsiflexion ROM = 0 at rest.

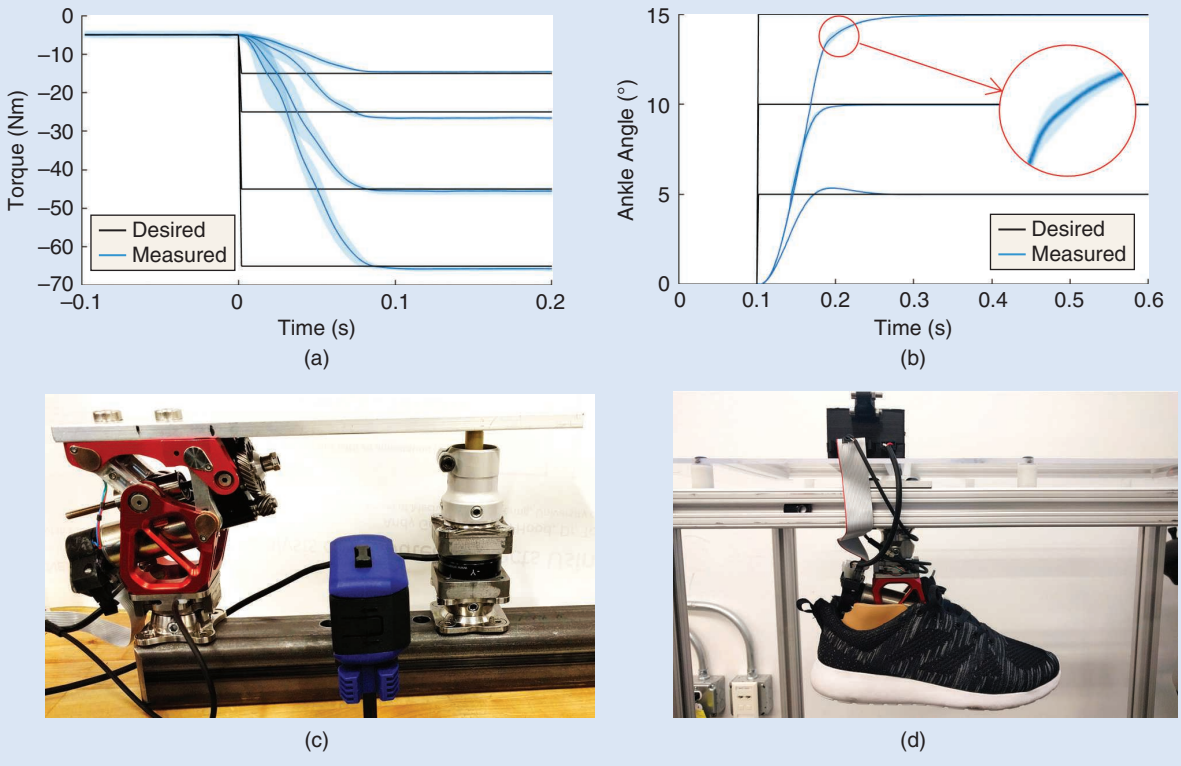

Figure 10. The results of the benchtop testing for the characterization of (a) the virtual impedance control and closed-loop position control, with (b) the standard deviation highlighted. (c) The benchtop testing setup for (d) the virtual impedance and position control.

height. Despite being capable of injecting net-positive energy into the gait cycle, the proposed polycentric powered prosthesis closely matches the weight of semiactive ankle-foot prostheses [10], [20], [34].

Experimental Validation

Benchtop Testing

To evaluate its torque performance, the device was rigidly attached to a steel frame at 0° with the foot keel resting against a six-axis load cell (Sunrise Instruments, M3713D) torque steps were commanded from a starting torque of −5 Nm [Figure 10(c)]. The load cell was used to compute torque at the ICR. Each step was conducted five times, and [Figure 10(a)] shows the mean and standard deviation of the measured torque at the ICR for each of the different step responses. The measured torque was zero-phase filtered in postprocessing at a cutoff frequency of 50 Hz. The mean and standard deviation of the step responses are displayed in Table 3. The mean rise times correspond to an estimated −3-dB bandwidth of 6.2, 7, 6.7, and 6.5 Hz for steps to −15, −25, −45, and −65 Nm, respectively. The bandwidth is calculated using $BW = 0.35/Tr$, where BW is the bandwidth and Tr is the rise time. This test suggests that the rise time and torque bandwidth of the system are comparable to those of previous studies and suitable for ambulation, as torque at the ankle joint during walking contains significant frequencies below 2 Hz [15].

Benchtop testing of the device was performed to assess the position tracking performance. Specifically, the device was attached to a rigid frame and commanded for five consecutive step responses, each from 0 to 5, 10, and 15° [Figure 10(d)]. The position data were recorded from the motor encoder and are unfiltered. Figure 10(b) shows the mean and standard deviation of the step responses. The mean rise time, 2% settling time, and steady-state error are displayed in Table 4. The estimated −3-dB bandwidth of the system is calculated to be 7.4, 7, and 5.3 Hz for the steps of 5, 10, and 15°, respectively, using $BW = 0.35/Tr$. This benchtop experiment demonstrates that the bandwidth of the position controller is appropriate for walking at a fast pace, because the bandwidth of the ankle joint position data for able-bodied individuals is characterized by significant frequencies at or below 2 Hz.

Biomechanical Assessment With Below-Knee Amputee Subjects

Subject Data and Experimental Methods

A demonstration of the powered polycentric ankle was provided by experiments involving two below-knee amputee subjects. The subjects' anthropometric data are given in Table 5. The ability of the powered ankle prothesis to assist users in walking and stair ascent was assessed by analyzing the ankle joint biomechanics for the powered prosthesis and the contralateral intact leg.

The experimental protocol was approved by the University of Utah's Institutional Review Board. Prior to the experiment, written informed consent was provided by the subjects as well as written permission to publish photos and videos of the experiments. None of the subjects had prior experience with a powered prothesis. At the beginning of the experimental session, the subjects wore the Xsens MVN, an IMU-based motion analysis system [51], to capture the walking- and stair-ascent kinematics while subjects wore their prescribed passive protheses. To this end, the subjects performed two 1-min walking sessions on a treadmill at the fixed speed of 1 m/s. Subsequently, they climbed stairs on a staircase that allows for two consecutive strides on the prosthesis side. For this test, the subjects ambulated

Table 3. A torque step response.

Step (Nm)	Rise Time (ms)	Steady-State Error (Nm)
−5 to −15	56.8 ± 1.1	0.4772 ± 0.070
−5 to −25	50 ± 2	−1.53 ± 0.41
−5 to −45	52.4 ± 3.6	−0.4402 ± 0.89
−5 to −65	54 ± 1.4	−0.532 ± 0.59

Table 4. A position step response.

Step (°)	Rise Time (ms)	Two-Percent Settling Time (ms)	Steady-State Error (°)
0 to 5	47.6 ± 0.89	241.6 ± 0.89	−0.0036 ± 0.0017
0 to 10	50 ± 2.4	191.2 ± 4.1	−0.0378 ± 0.0016
0 to 15	66.8 ± 3.9	248.4 ± 8.2	−0.0504 ± 0.0040

Table 5. The subject data.

Subject	Age (years)	Weight (kg)	Height (m)	Gender	Years Post-amputation	Cause of Amputation	Amputation Side	Prescribed Prosthesis
1	21	97.61	1.71	Female	8	Cancer	Left	Kinterra (Freedom Innovations)
2	26	72.6	1.79	Male	15	Trauma	Left	Challenger (Ottobock)

back and forth on the staircase at a self-selected cadence for 10 consecutive repetitions. Then, a certified prosthetist fitted the subjects with the powered polycentric ankle. The prosthetist was instructed to follow the same procedure normally used with commercially available prostheses, which consisted of adjusting the build height of the experimental prosthesis based on the subject's anthropometry and aligning the prosthesis joints to achieve comfortable and stable standing posture. Approximately 30 min of training with the powered polycentric ankle was provided to subjects prior to the data collection.

After the training was completed, the treadmill test was repeated [Figure 11(a)]. The test for stairs ambulation occurred on a staircase that allows for two consecutive strides on the prosthesis side [Figure 11(b)]. The subjects were asked to ambulate back and forth on the staircase at a self-selected cadence for 10 consecutive repetitions. Both tests consisted of the subject wearing the powered polycentric prosthesis. For the goal of this experiment, transitions between different ambulation modes were manually triggered by the experimenter using the GUI.

During the tests, we recorded signals from all the embedded prosthesis sensors at a sampling frequency of 500 Hz. During postprocessing, we divided the acquired data into separate strides using the outputs from the GRF sensors and the finite-state machine. Each recorded stride was normalized to the stride duration and resampled to 1,000 samples. Additionally, we normalized both the ICR and ankle joint torque to body weight. Finally, we computed the mean and standard deviations of the normalized ankle angle, ankle torque (measured using the instrumented pyramid), and ICR torque (estimated from motor current as previously done for ankle torque in [41]) profiles of all recorded strides and combined them for each subject.

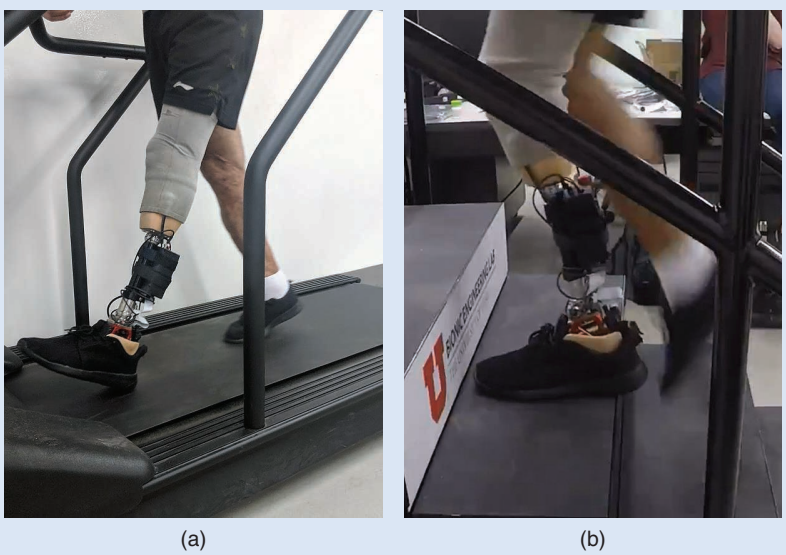

Figure 11. Still photos of subject 2 as he (a) walks on the treadmill and (b) ambulates on the staircase with the powered polycentric ankle.

Biomechanical Results

For both subjects, the powered ankle prosthesis provided kinematics and kinetics that qualitatively resemble the nominal walking profiles of able-bodied individuals. The average ankle kinematics and kinetics for each subject during the treadmill walking test are depicted in Figure 12. Positive angles and torques represent plantarflexion, whereas negative angles and torque represent dorsiflexion. Nominal kinematics and kinetics extracted from able-bodied individuals are shown using dashed red lines in all the panels. As seen in Figure 12(a) and (b), for both subjects, the powered ankle kinematics (solid blue lines) closely approximated the physiological ankle kinematics, including the peak plantarflexion angles in early stance and swing and the dorsiflexion angle in midstance; however, for subject 1 the latter was roughly 40% higher than that of the former.

Compared to the prescribed passive prostheses, the powered polycentric ankle produced a marked increase in ROM, especially in late stance and swing. Analysis of the ankle kinetics during walking [Figure 12(c) and (d)] shows a similar trend for the powered ankle prosthesis torque (blue lines) and the nominal able-bodied torque (red dashed lines). However, the peak torque of the powered prosthesis was roughly 20 and 28% lower than that of the nominal able-bodied trajectory for subjects 1 and 2, respectively. In agreement with the dynamic simulations (Figure 3), higher dorsiflexion torque and lower plantarflexion torque are seen at the ICR (solid orange line) compared to the ankle joint (solid blue line). Thus, the experimental data show that the proposed polycentric mechanism has the ability reduce the physiological plantarflexion torque bias, as predicted by our simulations.

The ability to inject net positive energy into the gait cycle is one of the key advantages of a powered prosthesis over a conventional passive prosthesis. While walking on the treadmill at 1 m/s, subject 1 had a self-selected cadence of 92 steps/min. During the walking tests, the powered polycentric ankle injected 10.1 ± 1.2 J/stride of mechanical energy, consuming 20.9 ± 1.7 J/stride of electrical energy. For subject 2, the self-selected cadence was ~96 steps/min. The powered ankle injected 8.6 ± 0.4 J/stride of mechanical energy, consuming 25.6 ± 1.2 J/stride of electrical energy. Interestingly, the observed mechanical energy injection matches that of previous experiments [52], where a powered ankle prosthesis was shown to reduce the metabolic cost of walking in seven individuals with below-knee amputations. However, the powered polycentric ankle is approximately 900 g lighter than the powered ankle used in [52], which may lead to further metabolic cost reductions [53]. With Wi-Fi and data recording on, the

electronic system required 3.8 W. As a result, the total electrical energy consumption during walking was 30.3 and 25.9 J/stride for subjects 1 and 2, respectively. In particular, the measured electrical energy consumption of the powered polycentric ankle is similar to that of heavier powered ankle prostheses using parallel springs [12], [13], [48]. Based on these data, the 1,050-mAh battery should enable subjects 1 and 2 to perform 5,525 and 6,480 walking steps, respectively, on a single battery charge, which meets our design objectives.

The average ankle kinematics and kinetics for the two subjects during the stair-ascent tests are shown in Figure 13. Positive angles and torques represent plantarflexion, whereas negative angles and torque represent dorsiflexion. Nominal kinematics and kinetics extracted from able-bodied individuals are presented using dashed red lines in all panels. The analysis of the ankle kinematics during stair ascent [Figure 13(a) and (b)] shows that the powered ankle (solid blue lines) approximates the nominal behavior of the ankle (dashed red lines), including an initial increase of the dorsiflexion angle, followed by a quick plantarflexion movement that starts in late stance and continues into early swing. Replicating this plantarflexion movement is particularly important because it leads to positive energy injection in late stance and improved toe clearance (early swing). This extended plantarflexion movement requires active control and therefore is not possible with a passive prosthesis.

Analysis of the ankle kinetics during stair ascent [Figure 13(c) and (d)] shows that the powered polycentric ankle can approximate the kinetic profile of the intact ankle, including a visible increase of ankle torque in late stance (40–60% of stride). However, as with the walking test, the peak of the ankle torque was lower for the powered polycentric ankle than that of the weight-matched, able-bodied ankle. Specifically, it was 46 and 23% lower for subjects 1 and 2, respectively. Among other factors, this disparity may be due to the slower cadence used by the subjects to climb our staircase, which has only four steps.

Although, the powered polycentric ankle was primarily optimized for walking, analysis of the ICR torque [orange lines in Figure 13(c) and (d)] shows that the polycentric

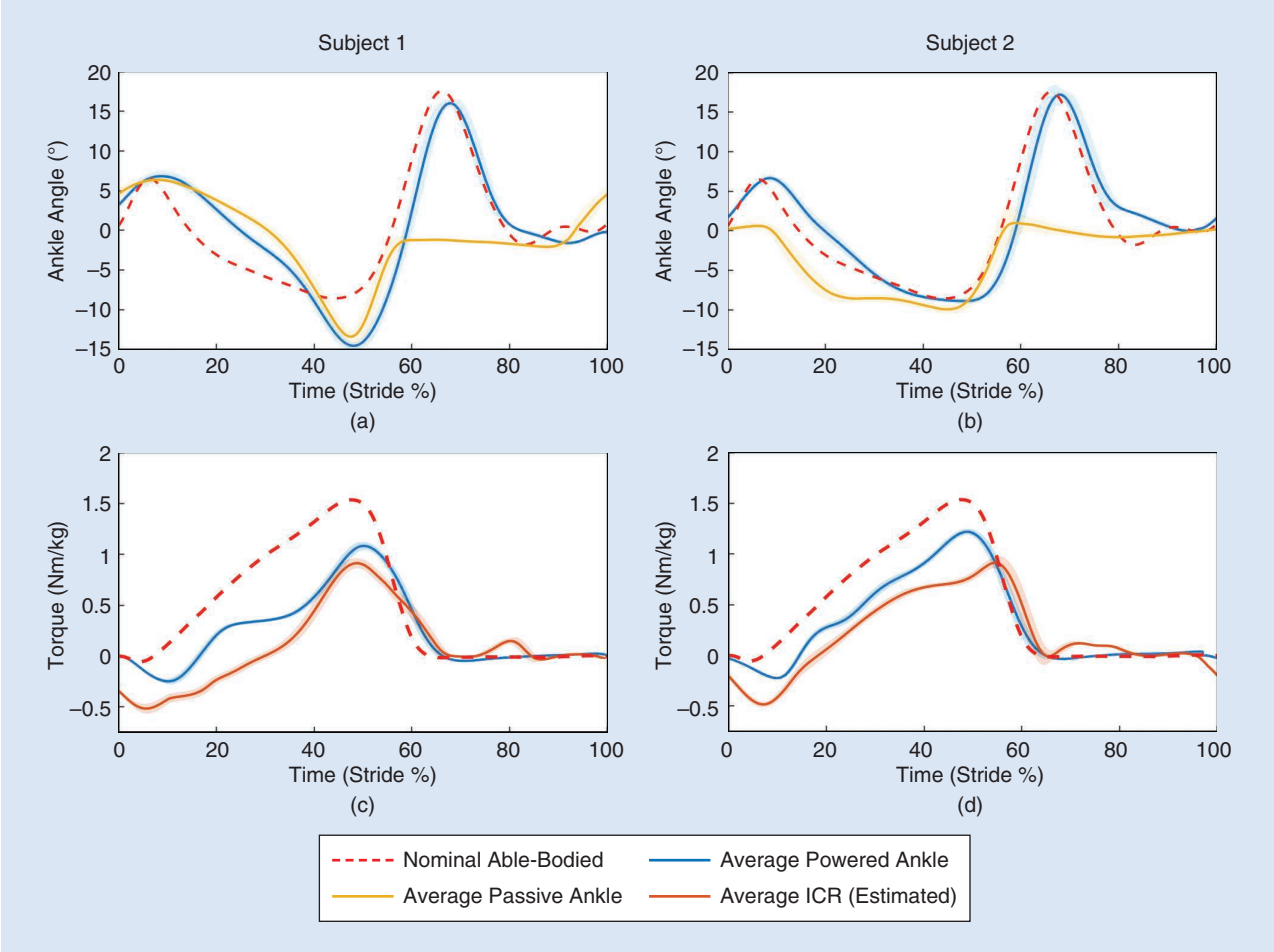

Figure 12. The (a) and (b) walking ankle kinematics and (c) and (d) kinetics for two below-knee amputee subjects using the powered polycentric ankle. Positive angles and torques represent plantarflexion and negative angles, respectively, and torque represents dorsiflexion. Ankle joint angles and torques for the powered polycentric ankle are shown with blue lines (mean) and shaded areas [standard deviation (STD)]. Ankle angles for the prescribed passive prosthesis are shown with yellow lines (mean) and shaded areas (STD). Orange lines (mean) and shaded areas (STD) represent the estimated torques at the ICR joint. Nominal kinematics and kinetics extracted from able-bodied individuals are shown with dashed red lines.

mechanism has a beneficial effect in stair ascent. Specifically, the peak of the ICR torque was 27 and 54% lower than that of the peak ankle torque for subjects 1 and 2, respectively. This experimental result agrees with the modeling, as both the CoP and the ICR location are anterior to the anatomical ankle location for the ankle angles seen in the stance phase during stair ascent. As expected from the analysis of intact leg kinetics [dashed red lines in Figure 13(c) and (d)], no dorsiflexion torque was observed in the stance phase during stair ascent. Thus, unlike walking, the absolute value of the ICR torque was lower than the absolute value of the ankle torque for the whole duration of stance.

Conclusions and Future Work

This article described the design and control of a powered polycentric prothesis for individuals with below-knee amputations. The proposed design aims to address the limitations of currently available powered ankle prostheses specifically related to build height and weight. The proposed powered prosthesis has 36.8% lower build height and is 40.9% lighter than the Ottobock, i.e., the only powered ankle-foot prosthesis on the market and complies with International Organization for Standardization standards. In addition, the proposed powered prosthesis is at least 40 and 45% smaller and lighter, respectively, than other research powered ankle-foot prostheses (Table 2). The smaller build height of the proposed design may enable more individuals with a below-knee amputation to use a powered ankle-foot prosthesis. Moreover, the lower weight of the proposed design, together with the ability to inject positive energy into the gait cycle, has the potential to improve the metabolic cost of walking [53].

The proposed powered ankle prosthesis was demonstrated on two below-knee amputee subjects walking on a treadmill and ascending stairs. The experimental results indicated that the biomechanical behavior of the powered polycentric ankle is representative of healthy ankle biomechanics. However, further studies are necessary to fully assess the efficacy of the proposed powered ankle on the broader amputee population. These studies should aspire to assess the biomechanical effects of the powered polycentric ankle on the residual

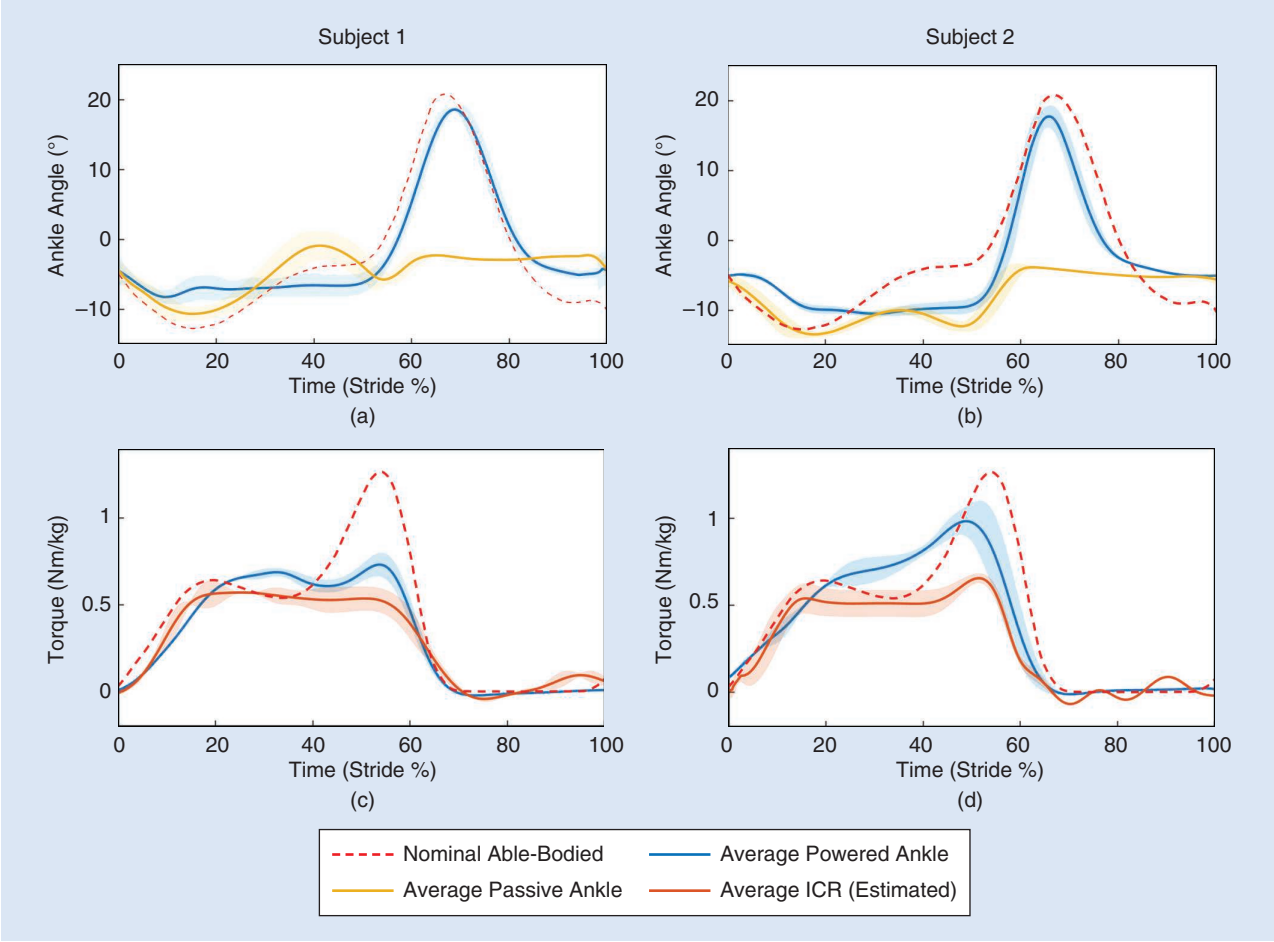

Figure 13. The (a) and (b) ankle kinematics and (c) and (d) kinetics for two below-knee amputee subjects using the powered polycentric ankle during stair ascent. Positive angles and torques represent plantarflexion and negative angles, respectively, and torque represents dorsiflexion. Ankle joint angles and torques for the powered polycentric ankle are shown with blue lines (mean) and shaded areas (STD). Ankle angles for the prescribed passive prosthesis are shown with yellow lines (mean) and shaded areas (STD). Orange lines (mean) and shaded areas (STD) represent the estimated torques at the ICR joint. Nominal kinematics and kinetics extracted from able-bodied individuals are represented by dashed red lines.

and contralateral leg as well as on the metabolic cost of ambulation. Future developmental work should also focus on improving the available controllers to better consider the effects of the polycentric mechanism on gait. These improvements may include closed-loop control based on the available ankle torque sensor and the implementation on quasi-stiffness curves [54] specific to the ICR in place of virtual impedance currently used. In addition, controllers for other ambulation activities (e.g., climbing ramps and performing sit-to-stand transitions) should be developed to fully assess the functional mobility with the powered polycentric ankle. To this end, automatic transitions between the different ambulation activities may be integrated using computer vision [43] or neural engineering approaches [55]. Finally, we plan to test the powered polycentric prosthesis in combination with a lightweight powered knee prosthesis [56] for individuals who have above-knee amputations.

References

[1] P. F. Adams, G. E. Hendershot, and M. A. Marano, "Current estimates from the National Health Interview Survey, 1996," *in Series 10: Data from the National Health Interview Survey,* no. 200, Atlanta, GA: Centers for Disease Control and Prevention, 1999, pp. 1–203.

[2] E. H. Sinitski, A. H. Hansen, and J. M. Wilken, "Biomechanics of the ankle–foot system during stair ambulation: Implications for design of advanced ankle–foot prostheses," *J. Biomech.*, vol. 45, no. 3, pp. 588–594, 2012.

[3] R. Versluys, P. Beyl, M. Van Damme, A. Desomer, R. Van Ham, and D. Lefeber, "Prosthetic feet: State-of-the-art review and the importance of mimicking human ankle-foot biomechanics," *Disabil. Rehabil. Assist. Technol.*, vol. 4, no. 2, pp. 65–75, 2009.

[4] E. Nickel, J. Sensinger, and A. Hansen, "Passive prosthetic ankle-foot mechanism for automatic adaptation to sloped surfaces," *J. Rehabil. Res. Dev.*, vol. 51, no. 5, pp. 803–814, 2014.

[5] A. Hahn, I. Sreckovic, S. Reiter, and M. Mileusnic, "First results concerning the safety, walking, and satisfaction with an innovative, microprocessor-controlled four-axes prosthetic foot," *Prosthet. Orthot. Int.*, vol. 42, no. 3, pp. 350–356, 2018. doi: 10.1177/0309364617747976.

[6] T. Lenzi, M. Cempini, J. Newkirk, L. J. Hargrove, and T. A. Kuiken, "A lightweight robotic ankle prosthesis with non-backdrivable cam-based transmission," in *Proc. Int. Conf. Rehabilitation Robotics (ICORR)*, 2017, pp. 1142–1147.

[7] T. Schmalz, S. Blumentritt, and R. Jarasch, "Energy expenditure and biomechanical characteristics of lower limb amputee gait: The influence of prosthetic alignment and different prosthetic components," *Gait Posture*, vol. 16, no. 3, pp. 255–263, 2002.

[8] N. T. Pickle, A. M. Grabowski, J. R. Jeffers, and A. K. Silverman, "The functional roles of muscles, passive prostheses, and powered prostheses during sloped walking in people with a transtibial amputation," *J. Biomech. Eng.*, vol. 139, no. 11, p. 111005, Nov. 2017. doi: 10.1115/1.4037938.

[9] M. Goldfarb, B. E. Lawson, and A. H. Shultz, "Realizing the promise of robotic leg prostheses," *Sci. Transl. Med.*, vol. 5, no. 210, pp. 210–215, 2013.

[10] Q. Wang, K. Yuan, J. Zhu, and L. Wang, "Walk the walk: A lightweight active transtibial prosthesis," *IEEE Robot. Autom. Mag.*, vol. 5, no. 210, p. 210ps15, Nov. 2015. doi: 10.1126/scitranslmed.3007312.

[11] R. D. Bellman, M. a. Holgate, and T. G. Sugar, "SPARKy 3: Design of an active robotic ankle prosthesis with two actuated degrees of freedom using regenerative kinetics," in *Proc. 2nd IEEE RAS EMBS Int. Conf. Biomedical Robotics Biomechatronics*, 2008, pp. 511–516.

[12] S. K. Au, J. Weber, and H. Herr, "Powered ankle—foot prosthesis improves walking metabolic economy," *IEEE Trans. Robot.*, vol. 25, no. 1, pp. 51–66, 2009.

[13] S. Au and H. Herr, "Powered ankle-foot prosthesis," *IEEE Robot. Autom. Mag.*, vol. 15, no. 3, pp. 52–59, 2008.

[14] B. Convens et al., "Modeling, design and test-bench validation of a semi-active propulsive ankle prosthesis with a clutched series elastic actuator," *IEEE Robot. Autom. Lett.*, vol. 4, no. 2, pp. 1823–1830, 2019.

[15] B. E. Lawson, J. Mitchell, D. Truex, A. Shultz, E. Ledoux, and M. Goldfarb, "A robotic leg prosthesis: design, control, and implementation," *IEEE Robot. Autom. Mag.*, vol. 21, no. 4, pp. 70–81, 2014.

[16] Össur, "Proprio foot." Accessed on: Sept. 9, 2019. [Online]. Available: https://www.ossur.com/prosthetic-solutions/products/dynamic-solutions/proprio-foot

[17] T. Lenzi, M. Cempini, L. Hargrove, and T. Kuiken, "Design, development, and testing of a lightweight hybrid robotic knee prosthesis," *Int. J. Robot. Res.*, vol. 37, no. 8, pp. 953–976, 2018.

[18] T. Lenzi, J. Sensinger, J. Lipsey, L. Hargrove, and T. Kuiken, "Design and preliminary testing of the RIC hybrid knee prosthesis," in *Proc. 37th Annu. Int. Conf. IEEE Engineering in Medicine and Biology Society (EMBS)*, 2015, pp. 1683–1686. doi: 10.1109/EMBC.2015.7318700.

[19] S. H. Collins and A. D. Kuo, "Recycling energy to restore impaired ankle function during human walking," *PLoS One*, vol. 5, no. 2, 2010. doi: 10.1371/journal.pone.0009307. [Online]. Available: https://journals.plos.org/plosone/article?id=10.1371/journal.pone.0009307

[20] T. Lenzi, M. Cempini, L. Hargrove, and T. Kuiken, "Design, development, and validation of a lightweight non-backdrivable robotic ankle prosthesis," *IEEE/ASME Trans. Mechatronics*, vol. 24, no. 2, pp. 471–482, Jan. 2019. doi: 10.1109/TMECH.2019.2892609.

[21] A. Baimyshev, B. Lawson, and M. Goldfarb, "Design and preliminary assessment of lightweight swing-assist knee prosthesis," in *Proc. 40th Annu. Int. Conf. IEEE Engineering in Medicine and Biology Society (EMBS)*, 2018, pp. 3198–3201.

[22] M. K. Shepherd and E. J. Rouse, "The VSPA foot: A quasi-passive ankle-foot prosthesis with continuously variable stiffness," *IEEE Trans. Neural Syst. Rehabil. Eng.*, vol. 25, no. 12, pp. 2375–2386, 2017.

[23] J. D. Smith and P. E. Martin, "Effects of prosthetic mass distribution on metabolic costs and walking symmetry," *J. Appl. Biomech.*, vol. 29, no. 3, pp. 317–328, 2013.

[24] J. D. Smith and P. E. Martin, "Short and longer term changes in amputee walking patterns due to increased prosthesis inertia," *JPO J. Prosthet. Orthot.*, vol. 23, no. 3, pp. 114–123, 2011.

[25] Y. Narang, V. Arelekatti, and A. Winter, "The effects of prosthesis inertial properties on prosthetic knee moment and hip energetics required to achieve able-bodied kinematics," *IEEE Trans. Neural Syst. Rehabil. Eng.*, vol. 24, no. 7, pp. 754–763, 2015.

[26] M. P. Aragon, G. A. V. Orozco, and A. A. Altamirano, "Bionic hip prosthesis based on polycentric mechanisms," in *Proc. Pan American Health Care Exchanges (PAHCE)*, 2013, pp. 1–5. doi: 10.1109/PAHCE.2013.6568260.

[27] L. Xu, D.-H. Wang, Q. Fu, G. Yuan, and L.-Z. Hu, "A novel four-bar linkage prosthetic knee based on magnetorheological effect: Principle, structure, simulation and control," *Smart Mater. Struct.*, vol. 25, no. 11, p. 115,007, 2016.

[28] A. K. Laprè, B. R. Umberger, and F. C. Sup, "A robotic ankle-foot prosthesis with active alignment," *ASME J. Med. Devices*, vol. 10, no. 2, p. 025001, 2016. doi: 10.1115/1.4032866.

[29] M. Cempini, L. J. Hargrove, and T. Lenzi, "Design, development, and bench-top testing of a powered polycentric ankle prosthesis," in *Proc. IEEE/RSJ Int. Conf. Intelligent Robots and Systems*, 2017, pp. 1064–1069.

[30] G. Bovi, M. Rabuffetti, P. Mazzoleni, and M. Ferrarin, "A multiple-task gait analysis approach: Kinematic, kinetic and EMG reference data for healthy young and adult subjects," *Gait Posture*, vol. 33, no. 1, pp. 6–13, 2011.

[31] D. A. Winter, "Appendix A" in *Biomechanics and Motor Control of Human Movement*, 4th ed. New York: Wiley, 2009, pp. 341–349.

[32] R. Riener, M. Rabuffetti, and C. Frigo, "Stair ascent and descent at different inclinations," *Gait Posture*, vol. 15, no. 1, pp. 32–44, 2002.

[33] P. Cherelle, V. Grosu, A. Matthys, B. Vanderborght, and D. Lefeber, "Design and validation of the ankle mimicking prosthetic (AMP-) foot 2.0," *IEEE Trans. Neural Syst. Rehabil. Eng.*, vol. 22, no. 1, pp. 138–148, 2014.

[34] M. Alimusaj, L. Fradet, F. Braatz, H. J. Gerner, and S. I. Wolf, "Kinematics and kinetics with an adaptive ankle foot system during stair ambulation of transtibial amputees," *Gait Posture*, vol. 30, no. 3, pp. 356–363, 2009.

[35] R. Drillis, R. Contini, and M. Bluestein, "Body segment parameters: A survey of measurement techniques," *Artif. Limbs*, vol. 8, pp. 44–66, Dec. 1964.

[36] Ottobock, "Empower." [Online]. Accessed on Sept. 9, 2019. Available: https://www.ottobockus.com/prosthetics/lower-limb-prosthetics/solution-overview/empower-ankle/

[37] D. R. Bassett, H. R. Wyatt, H. Thompson, J. C. Peters, and J. O. Hill, "Pedometer-measured physical activity and health behaviors in U.S. adults," *Med. Sci. Sports Exerc.*, vol. 42, no. 10, pp. 1819–1825, 2010.

[38] A. LaPrè and F. Sup, "A control strategy for an active alignment transtibial prosthesis," in *Proc. ASME Dynamic Systems and Control Conf.*, 2015, p. V001T18A005. doi: 10.1115/DSCC2015-9948.

[39] J. W. Sensinger, N. Intawachirarat, and S. A. Gard, "Contribution of prosthetic knee and ankle mechanisms to swing-phase foot clearance," *IEEE Trans. Neural Syst. Rehabil. Eng.*, vol. 21, no. 1, pp. 74–80, 2013.

[40] L. Gabert and T. Lenzi, "Instrumented pyramid adapter for amputee gait analysis and powered prosthesis control," *IEEE Sens. J.*, vol. 19, no. 18, pp. 8272–8282, 2019.

[41] A. J. Young, A. M. Simon, and L. J. Hargrove, "A training method for locomotion mode prediction using powered lower limb prostheses," *IEEE Trans. Neural Syst. Rehabil. Eng.*, vol. 22, no. 3, pp. 671–677, 2014.

[42] H. Huang, F. Zhang, L. J. Hargrove, Z. Dou, D. R. Rogers, and K. B. Englehart, "Continuous locomotion-mode identification for prosthetic legs based on neuromuscular–mechanical fusion," *IEEE Trans. Biomed. Eng.*, vol. 58, no. 10, pp. 2867–2875, 2011.

[43] N. E. Krausz, T. Lenzi, and L. J. Hargrove, "Depth sensing for improved control of lower limb prostheses," *IEEE Trans. Biomed. Eng.*, vol. 62, no. 11, pp. 2576–2587, 2015.

[44] T. Lenzi, L. Hargrove, and J. W. Sensinger, "Preliminary evaluation of a new control approach to achieve speed adaptation in robotic transfemoral prostheses," in *Proc. IEEE/RSJ Int. Conf. Intelligent Robots and Systems*, 2014, pp. 2049–2054.

[45] K. Shamaei, G. S. Sawicki, and A. M. Dollar, "Estimation of quasi-stiffness and propulsive work of the human ankle in the stance phase of walking," *PLoS One*, vol. 8, no. 3, 2013. doi: 10.1371/journal.pone.0059935. [Online]. Available: https://journals.plos.org/plosone/article?id=10.1371/journal.pone.0059935

[46] T. Lenzi, L. J. Hargrove, and J. W. Sensinger, "Minimum jerk swing control allows variable cadence in powered transfemoral prostheses," in *Proc. IEEE 36th Annu. Int. Conf. Engineering in Medicine and Biology Society*, 2014, pp. 2492–2495.

[47] G. Aguirre-Ollinger, J. E. Colgate, M. A. Peshkin, and A. Goswami, "Design of an active one-degree-of-freedom lower-limb exoskeleton with inertia compensation," *Int. J. Robot. Res.*, vol. 30, no. 4, pp. 486–499, 2011.

[48] A. H. Shultz, B. E. Lawson, and M. Goldfarb, "Variable cadence walking and ground adaptive standing with a powered ankle prosthesis," *IEEE Trans. Neural Syst. Rehabil. Eng.*, vol. 24, no. 4, pp. 495–505, 2016.

[49] M. Grimmer et al., "A powered prosthetic ankle joint for walking and running," *Biomed. Eng. Online*, vol. 15, p. 286, Dec. 2016.

[50] B. J. Darter and J. M. Wilken, "Energetic consequences of using a prosthesis with adaptive ankle motion during slope walking in persons with a transtibial amputation," *Prosthet. Orthot. Int.*, vol. 38, no. 1, pp. 5–11, 2014.

[51] J.-T. Zhang, A. C. Novak, B. Brouwer, and Q. Li, "Concurrent validation of Xsens MVN measurement of lower limb joint angular kinematics," *Physiol. Meas.*, vol. 34, no. 8, pp. N63–N69, 2013.

[52] H. M. Herr and A. M. Grabowski, "Bionic ankle-foot prosthesis normalizes walking gait for persons with leg amputation," *Proc. Roy. Soc. B Biol. Sci.*, vol. 279, no. 1728, pp. 457–464, 2012.

[53] R. C. Browning, J. R. Modica, R. Kram, and A. Goswami, "The effects of adding mass to the legs on the energetics and biomechanics of walking," *Med. Sci. Sports Exerc.*, vol. 39, no. 3, pp. 515–525, 2007.

[54] T. Lenzi, L. Hargrove, and J. Sensinger, "Speed-adaptation mechanism: Robotic prostheses can actively regulate joint torque," *IEEE Robot. Autom. Mag.*, vol. 21, no. 4, pp. 94–107, 2014.

[55] L. J. Hargrove, et al. "Intuitive control of a powered prosthetic leg during ambulation: A randomized clinical trial," *JAMA*, vol. 313, no. 22, pp. 2244–2252, 2015.

[56] M. Tran, L. Gabert, M. Cempini, and T. Lenzi, "A lightweight, efficient fully powered knee prosthesis with actively variable transmission," *IEEE Robot. Autom. Lett.*, vol. 4, no. 2, pp. 1186–1193, 2019.

Lukas Gabert, Department of Mechanical Engineering and Utah Robotics Center, University of Utah, Salt Lake City. Email: lukas.r.gabert@utah.edu.

Sarah Hood, Department of Mechanical Engineering and Utah Robotics Center, University of Utah, Salt Lake City. Email: sarah.hood@utah.edu.

Minh Tran, Department of Mechanical Engineering and Utah Robotics Center, University of Utah, Salt Lake City. Email: mqtran1512@gmail.com.

Marco Cempini, Neocis Inc., Miami, Florida. Email: mcempini@gmail.com.

Tommaso Lenzi, Department of Mechanical Engineering and Utah Robotics Center, University of Utah, Salt Lake City. Email: t.lenzi@utah.edu.